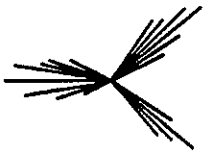

Instituto de Física Teórica
Universidade Estadual Paulista

August /93

IFT–P.053/93
IFUSP-P 1065

Triple Vector Boson Processes in $\gamma\gamma$ Colliders

F. T. Brandt [a], O. J. P. Éboli [a], E. M. Gregores [b],
M. B. Magro [a], P. G. Mercadante [a], and S. F. Novaes [b]

[a] *Instituto de Física,*
Universidade de São Paulo,
C.P. 20516, 01498-970 São Paulo,
Brazil

[b] *Instituto de Física Teórica,*
Universidade Estadual Paulista,
Rua Pamplona 145, 01405-900 São Paulo,
Brazil

Instituto de Física Teórica
Universidade Estadual Paulista
Rua Pamplona, 145
01405-900 – São Paulo, S.P.
Brazil

Telephone: 55 (11) 251-5155
Telefax: 55 (11) 288-8224
Telex: 55 (11) 31870 UJMFBR
Electronic Address: LIBRARY@IFT.UESP.ANSP.BR
47553::LIBRARY

IFT-P.053/93 and IFUSP-P 1065

Triple Vector Boson Processes in $\gamma\gamma$ Colliders

F. T. Brandt [a], O. J. P. Éboli [a], E. M. Gregores [b],

M. B. Magro [a], P. G. Mercadante [a], and S. F. Novaes [b]

[a] *Instituto de Física, Universidade de São Paulo,*

C.P. 20516, 01498-970 São Paulo, Brazil

[b] *Instituto de Física Teórica, Universidade Estadual Paulista,*

Rua Pamplona 145, 01405-900 São Paulo, Brazil.

(September 10, 1993)

Abstract

We study the production of three gauge bosons at the next generation of linear e^+e^- colliders operating in the $\gamma\gamma$ mode. The processes $\gamma\gamma \to W^+W^-V$ ($V = Z^0$, or γ) can provide direct information about the quartic gauge-boson couplings. We analyze the total cross section as well as several dynamical distributions of the final state particles including the effect of kinematical cuts. We find out that a linear e^+e^- machine operating in the $\gamma\gamma$ mode will produce 5–10 times more three-gauge-boson states compared to the standard e^+e^- mode at high energies.

I. INTRODUCTION

The multiple vector-boson production will be a crucial test of the gauge structure of the Standard Model since the triple and quartic vector-boson couplings involved in this kind of reaction are strictly constrained by the $SU(2)_L \otimes U(1)_Y$ gauge invariance. Any small deviation from the Standard Model predictions for these couplings spoils the intimate cancellations of the high energy behaviour between the various diagrams, giving rise to an anomalous growth of the cross section with energy. It is important to measure the vector-boson selfcouplings and look for deviations from the Standard Model, which would provide indications for a new physics.

The production of several vector bosons is the ideal place to search directly for any anomalous behaviour of the triple and quartic couplings. The reaction $e^+e^- \to W^+W^-$ will be accessible at LEP200 and important information about the $WW\gamma$ and WWZ vertices will be available in the near future [1]. Nevertheless, due to its limited center of mass energy available, we will have to wait for colliders with higher center of mass energy in order to produce a final state with three or more gauge bosons and to test the quartic gauge-boson coupling. The measurement of the three-vector-boson production cross section can provide a non-trivial test of the Standard Model that is complementary to the analyses of the production of vector-boson pairs. Previously, the cross sections for triple gauge boson production in the framework of the Standard Model were presented for e^+e^- colliders [2–4] and hadronic colliders [2,5].

An interesting option that is deserving a lot of attention nowadays is the possibility of transforming a linear e^+e^- collider in a $\gamma\gamma$ collider. By using the old idea of Compton laser backscattering [6], it is possible to obtain very energetic photons from an electron or positron beam. The scattering of a laser with few GeV against a electron beam is able to give rise to a scattered photon beam carrying almost all the parent electron energy with similar luminosity of the electron beam [7]. This mechanism can be employed in the next generation of e^+e^- linear colliders [8,9] (NLC) which will reach a center of mass energy of

500–2000 GeV with a luminosity of $\sim 10^{33}$ cm^{-2} s^{-1}. Such machines operating in $\gamma\gamma$ mode will be able to study multiple vector boson production with high statistic.

In this work, we examine the production of three vector bosons in $\gamma\gamma$ collisions through the reactions

$$\gamma + \gamma \to W^+ + W^- + Z^0 \,, \tag{I}$$

$$\gamma + \gamma \to W^+ + W^- + \gamma \,. \tag{II}$$

These processes involve only interactions of between the gauge bosons making more evident any deviation from predictions of the Standard Model gauge structure. Besides that, there is no tree-level contribution involving the Higgs boson which eludes all the uncertainties coming from the scalar sector, like the Higgs boson mass. Nevertheless, the production of multiple longitudinal gauge bosons can shed light on the symmetry breaking mechanism even when there is no contribution coming from the standard Higgs boson. For instance, in models where the electroweak-symmetry breaking sector is strongly interacting there is an enhancement of this production [5,10].

We analyze the total cross section of the processes above, as well as the dynamical distributions of the final state vector bosons. We concentrate on final states where the W and Z^0 decay into identifiable final states. We conclude that for a center of mass energy $\sqrt{s} \gtrsim 500$ GeV and an annual integrated luminosity of 10 fb^{-1}, there will be a promising number of fully reconstructible events. Moreover, we find out that a linear e^+e^- machine operating in the $\gamma\gamma$ mode will produce 5–10 times more three-gauge-boson states compared to the standard e^+e^- mode at high energies.

The outline is as follows. In Sec. II, we introduce the laser backscattering spectrum, and present the details of the calculational method. Section III contains our results for the total cross section and the kinematical distributions of the final state gauge bosons for center of mass energies $\sqrt{s} = 0.5$ and 1 TeV. This paper is supplemented by an appendix which gives the invariant amplitudes for the above processes.

II. CALCULATIONAL METHOD

The cross section for the triple-vector-boson production via $\gamma\gamma$ fusion can be obtained by folding the elementary cross section for the subprocesses $\gamma\gamma \to WWV$ ($V = Z^0,\ \gamma$) with the photon luminosity ($dL_{\gamma\gamma}/dz$),

$$d\sigma(e^+e^- \to \gamma\gamma \to WWV)(s) = \int_{z_{\min}}^{z_{\max}} dz\ \frac{dL_{\gamma\gamma}}{dz}\ d\hat{\sigma}(\gamma\gamma \to WWV)(\hat{s} = z^2 s)\ , \qquad (1)$$

where $\sqrt{s}$ ($\sqrt{\hat{s}}$) is the e^+e^- ($\gamma\gamma$) center of mass energy and $z^2 = \tau \equiv \hat{s}/s$. Assuming that the whole electron beam is converted into photons via the laser backscattering mechanism, the relation connecting the photon structure function $F_{\gamma/e}(x,\xi)$ to the photon luminosity is

$$\frac{dL_{\gamma\gamma}}{dz} = 2\sqrt{\tau}\ \int_{\tau/x_{\max}}^{x_{\max}} \frac{dx}{x} F_{\gamma/e}(x,\xi) F_{\gamma/e}(\tau/x,\xi)\ . \qquad (2)$$

For unpolarized beams the photon-distribution function [7] is given by

$$F_{\gamma/e}(x,\xi) \equiv \frac{1}{\sigma_c}\frac{d\sigma_c}{dx} = \frac{1}{D(\xi)}\left[1 - x + \frac{1}{1-x} - \frac{4x}{\xi(1-x)} + \frac{4x^2}{\xi^2(1-x)^2}\right]\ , \qquad (3)$$

with

$$D(\xi) = \left(1 - \frac{4}{\xi} - \frac{8}{\xi^2}\right)\ln(1+\xi) + \frac{1}{2} + \frac{8}{\xi} - \frac{1}{2(1+\xi)^2}\ , \qquad (4)$$

where σ_c is the Compton cross section, $\xi \simeq 4E\omega_0/m_e^2$, m_e and E are the electron mass and energy respectively, and ω_0 is the laser-photon energy. The fraction x represents the ratio between the scattered photon and initial electron energy for the backscattered photons traveling along the initial electron direction. The maximum value of x is

$$x_{\max} = \frac{\omega_{\max}}{E} = \frac{\xi}{1+\xi}\ , \qquad (5)$$

with $\omega_{\max}$ being the maximum scattered photon energy.

The fraction of photons with energy close to the maximum value grows with $\sqrt{s}$ and ω_0. Nevertheless, the bound $\xi < 2(1+\sqrt{2})$ should be respected in order to avoid the reduction in the efficiency of the $e \to \gamma$ conversion due to the creation of e^+e^- pairs in collisions of the laser with backscattered photons. We assumed that ω_0 has the maximum value compatible

with the above constraint, *e.g.* for $\sqrt{s} = 500$ GeV, $\omega_0 = 1.26$ eV and $x_{\max} \simeq 0.83$. With this choice, more than half of the scattered photons are emitted inside a small angle ($\theta < 5 \times 10^{-6}$ rad) and carry a large amount of the electron energy. Due to this hard photon spectrum, the luminosity Eq. (2) is almost constant for $z < x_{\max}$.

The analytical calculation of the cross section for the process $\gamma\gamma \to W^+W^-\gamma$ ($\gamma\gamma \to W^+W^-Z^0$) requires the evaluation of twelve Feynman diagrams in the unitary gauge, which is a tedious and lengthy calculation despite of being straightforward. For the sake of completeness, we exhibit in the Appendix the expression of the amplitudes of these processes. In order to perform these calculations in a efficient and reliable way [11], we used an improved version of the numerical technique presented in Ref. [3,12]. The integrations were also performed numerically using a Monte Carlo routine [13] and we tested the Lorentz and $U(1)_{em}$ gauge invariances of our results for the amplitudes.

III. CROSS SECTIONS AND GAUGE-BOSON DISTRIBUTIONS

We have evaluated the total cross section for the processes $\gamma\gamma \to W^+W^-V$ imposing kinematical cuts on the final state particles. Our first cut required that the produced gauge bosons are in the central region of the detector, *i.e.* we imposed that the angle of vector boson with the beam pipe is larger than 30°, which corresponds to a cut in the pseudo-rapidity of $|\eta| < 1.32$. We further required the isolation of the final particles by demanding that all vector bosons make an angle larger than 25° between themselves. Moreover, for the process II, we imposed a cut on the photon transverse momentum, $p_T^\gamma > 10$ GeV, to guarantee that the results are free of infrared divergences and to mimic the performance of a typical electromagnetic calorimeter.

In Tables I and II we exhibit the results for the total cross section of the processes I and II, with and without the above cuts. As we can see from these tables, the two-gauge-boson cross section ($\gamma + \gamma \to W^+ + W^-$), which is the main reaction in a $\gamma\gamma$ collider [14], is from 2 to 4 orders of magnitude above those for three gauge bosons depending upon

$\sqrt{s}$. Nevertheless, we still find promising event rates for final states W^+W^-V for an e^+e^- collider with an annual integrated luminosity of 10 fb^{-1}. Moreover, the triple-gauge-boson production in e^+e^- and $\gamma\gamma$ colliders are comparable at $\sqrt{s} = 500$ GeV, while the event rate in $\gamma\gamma$ collider is a factor of 5–10 larger than the one in a e^+e^- machine at $\sqrt{s} = 1$ TeV. The observed growth of the total cross section for the production of three gauge bosons is due to gauge-boson exchange in the t and u channels.

Since we are interested in final states where all the gauge bosons are identified, the event rate is determined not only by the total cross section, but also by the reconstruction efficiency that depends on the particular decay channels of the vector bosons. In principle, charged lepton and light quark jet pairs can be easily identified. However, in the semileptonic decay of heavy quark the presence of unmeasurable neutrinos spoils the invariant mass measurement, and we adopt, as in Ref. [3], that the efficiency for reconstruction of a $W^\pm$ (Z^0) is 0.61 (0.65). In general, final-state photons can be identified with high efficiency as an electromagnetic shower with a neutral initiator. Combining the reconstruction efficiencies for individual particles, we obtain that the process I (II) has a detection efficiency of 0.24 (0.37). Once the reconstruction efficiency is substantial, the crucial factor for event rates is the production cross section. Assuming the above cuts and efficiencies we expect, for a 500 (1000) GeV collider with an annual integrated luminosity of 10 fb^{-1}, a total yield of 25 (198) $\gamma + \gamma \to W^+ + W^- + Z^0$ fully reconstructed events per year and 428 (714) $\gamma + \gamma \to W^+ + W^- + \gamma$ reconstructed events per year with $P_T^\gamma > 10$ GeV.

In order to reach a better understanding of these reactions, we present in Fig. 1–6 various distributions of the final state gauge bosons. In Fig. 1 we show the distribution in $\cos\theta$, where θ is the polar angle of the particles ($W^\pm$, and $V = \gamma, Z^0$) with the beam pipe. The results are presented with and without the angular cuts described above. The W^+ and W^- curves coincide due to the charge conjugation invariance. We should notice that these processes are particularly sensitive to central region requirement since, analogously to what happens in the reaction $\gamma\gamma \to W^+W^-$, the W's go preferentially along the beam pipe direction. This fact can also be seen from the rapidity distribution of the final state

particles (Fig. 2). Therefore, the requirement that the gauge bosons are produced in the central region of the detector implies in a loss of 1/2 to 5/6 of the total number of events. Increasing the center of mass energy, the W's tend to populate the high rapidity region while the $V = \gamma, Z^0$ distribution maintains its shape. Consequently, the cut in the W angle with beam pipe discards most of the high energy events.

In order to estimate the importance of the isolation cut on the final particles, we present in Fig. 3 the distributions in the angle between the vector bosons. Charge conjugation invariance of the processes implies that the distribution for W^+Z^0 and W^-Z^0 are the same. In both processes I and II, the W's tend to be back-to-back, while the WV ($V = Z^0$ or γ) is relatively flat, demonstrating that the isolation cut is not very restrictive. The distribution for different energies of the collider are quite similar, apart from a constant factor due to the growth of the total cross section.

The invariant mass distributions of the W^+W^- and $W^\pm Z^0$ (γ) pairs are presented in Fig. 4. Once again the W^+Z^0 (γ) and W^-Z^0 (γ) curves coincide. From this Figure we can learn that the average invariant mass of the pairs W^+W^- is higher then the one for WZ^0 (γ) pairs. As the center of mass energy of the collider is increased the distributions grows due to the growth of the total cross section. Moreover, the invariant mass distribution for WZ^0 (γ) and W^+W^- pairs are considerably different: the former is rather narrow and peaked at small invariant masses while the later one is broader and peaked at high invariant masses.

Figure 5 shows the laboratory energy distributions the of the $W^\pm$ and Z^0 (γ) gauge bosons. In the process $\gamma\gamma \to W^+W^-Z^0$, the E_Z and $E_{W^\pm}$ distributions are rather similar, with the average energy of the $W^\pm$ being larger than the average Z^0 energy. As the center of mass energy of the collider is increased the distributions grow and become rather isolated, while the peaks broaden systematically. In the process $\gamma\gamma \to W^+W^-\gamma$, the distributions in E_γ and $E_{W^\pm}$ are very different due to the infrared divergences: the E_γ is strongly peaked towards small energies while $E_{W^\pm}$ is rather broad and peaked at high energies. With the increase of the collider energy the difference between the distribution become clearer.

We exhibit in Fig. 6 the transverse-momentum distribution for the $W^{\pm}$ and Z^0 (γ) vector bosons. There are no distinctive difference between the distribution for $W^{\pm}$ and Z^0 in process I, apart from the fact that the Z^0's exhibit a smaller average p_T than the W's. In the case of process II, the distributions for γ and $W^{\pm}$ are very different since the first is peaked at very small p_T due to the infrared divergences.

Note added. After completing this work, we came across an estimate of the total elementary cross section for the processes studied here done by M. Baillargeon and F. Boudjema [15].

ACKNOWLEDGMENTS

This work was partially supported by Conselho Nacional de Desenvolvimento Científico e Tecnológico (CNPq), and by Fundação de Amparo à Pesquisa do Estado de São Paulo (FAPESP).

APPENDIX

We collect in this appendix the expressions for the amplitudes of the processes $\gamma\gamma \to W^+W^-V$, with $V = Z^0$ or γ. The Feynman diagrams contributing to these processes are given in Fig. 7. The momenta and polarizations of the initial photons where denoted by (k_1, k_2) and ($\epsilon_\mu(k_1)$, $\epsilon_\nu(k_2)$), while the momenta and polarizations of the final state W^+, W^- and V are given by (p_+, p_-, k_3) and ($\epsilon_\alpha(p_+)$, $\epsilon_\beta(p_-)$, $\epsilon_\gamma(k_3)$) respectively. For a given choice of the initial and final polarizations the amplitude of these processes can be written as

$$M = G_v \epsilon_\mu(k_1)\epsilon_\nu(k_2)\epsilon_\alpha(p_+)\epsilon_\beta(p_-)\epsilon_\gamma(k_3) M_T^{\mu\nu\alpha\beta\gamma} , \tag{A1}$$

with

$$M_T^{\mu\nu\alpha\beta\gamma} = \sum_{i=1}^{7} M_i^{\mu\nu\alpha\beta\gamma} , \tag{A2}$$

where the $M_i^{\mu\nu\alpha\beta\gamma}$ is the contribution of the set of diagrams i to the processes. The factor G_v depends upon the process, assuming the value e^3 for the production of $W^+W^-\gamma$ and the value $e^3 \cot^2\theta_W$, with θ_W being the Weinberg angle, for the final state $W^+W^-Z^0$.

In order to write a compact expression for the amplitude, it is convenient to define the triple-gauge-boson coupling coefficient as

$$\Gamma_3^{\alpha\beta\gamma}(P_1,P_2) = \left[(2P_1+P_2)^\beta g^{\alpha\gamma} - (2P_2+P_1)^\alpha g^{\beta\gamma} + (P_2-P_1)^\gamma g^{\beta\alpha}\right] , \tag{A3}$$

the quartic-gauge-boson coupling

$$\Gamma_4^{\mu\nu\alpha\beta} = g^{\mu\alpha}g^{\nu\beta} + g^{\mu\beta}g^{\nu\alpha} - 2g^{\mu\nu}g^{\alpha\beta} , \tag{A4}$$

and the propagator tensor

$$D^{\mu\nu}(k) = \frac{(g^{\mu\nu} - k^\mu k^\nu/m^2)}{k^2 - m^2} . \tag{A5}$$

Using the above definitions, the contributions of the different set of diagrams can be written as

$$\begin{aligned} M_1^{\mu\nu\alpha\beta\gamma} = {} & \Gamma_3^{\alpha\gamma\xi}(p_+,k_3) D_{\xi\sigma}(p_+ + k_3) \Gamma_3^{\mu\sigma\rho}(k_1, -(p_+ + k_3)) \\ & D_{\rho\lambda}(p_- - k_2) \Gamma_3^{\beta\nu\lambda}(-p_-, k_2) + \ [k_{1\leftrightarrow 2}\ ;\ \mu \leftrightarrow \nu] \end{aligned} \tag{A6}$$

$$\begin{aligned} M_2^{\mu\nu\alpha\beta\gamma} = {} & \Gamma_3^{\alpha\beta\xi}(k_3,p_-) D_{\xi\sigma}(p_- + k_3) \Gamma_3^{\sigma\nu\rho}(-p_- - k_3, k_2) \\ & D_{\rho\lambda}(k_1 - p_+) \Gamma_3^{\mu\alpha\lambda}(-p_+, k_2) + \ [k_{1\leftrightarrow 2}\ ;\ \mu \leftrightarrow \nu] \end{aligned} \tag{A7}$$

$$\begin{aligned} M_3^{\mu\nu\alpha\beta\gamma} = {} & \Gamma_3^{\mu\alpha\xi}(k_1, -p_+) D_{\xi\sigma}(k_1 - p_+) \Gamma_3^{\gamma\sigma\rho}(-k_3, (k_1 - p_+)) \\ & D_{\rho\lambda}(p_- - k_2) \Gamma_3^{\nu\beta\lambda}(-k_2, p_-) + \ [k_{1\leftrightarrow 2}\ ;\ \mu \leftrightarrow \nu] \end{aligned} \tag{A8}$$

$$M_4^{\mu\nu\alpha\beta\gamma} = \Gamma_3^{\beta\nu\xi}(-p_-, k_2) D_{\xi\lambda}(k_2 - p_-) \Gamma_4^{\lambda\alpha\mu\gamma} + \ [k_{1\leftrightarrow 2}\ ;\ \mu \leftrightarrow \nu] \tag{A9}$$

$$M_5^{\mu\nu\alpha\beta\gamma} = \Gamma_3^{\mu\alpha\xi}(k_1, -p_+) D_{\xi\lambda}(k_1 - p_+) \Gamma_4^{\lambda\beta\nu\gamma} + \ [k_{1\leftrightarrow 2}\ ;\ \mu \leftrightarrow \nu] \tag{A10}$$

$$M_6^{\mu\nu\alpha\beta\gamma} = \Gamma_3^{\alpha\gamma\xi}(p_+,k_3) D_{\xi\lambda}(p_+ + k_3) \Gamma_4^{\lambda\beta\nu\mu} \tag{A11}$$

$$M_7^{\mu\nu\alpha\beta\gamma} = \Gamma_3^{\gamma\beta\xi}(k_3,p_-) D_{\xi\lambda}(-p_- - k_3) \Gamma_4^{\lambda\alpha\nu\mu} \tag{A12}$$

where $[k_{1\leftrightarrow 2}\ ;\ \mu \leftrightarrow \nu]$ indicates the crossed contributions of the initial photons.

REFERENCES

[1] K. Hagiwara, R. D. Peccei, D. Zeppenfeld, and K. Hikasa, Nucl. Phys. **B282**, 253 (1987); Proceedings of the ECFA Workshop on LEP200, CERN Report 87-08, ECFA Report 87/108, ed. A. Böhm and W. Hoogland, Aachen 1987.

[2] V. Barger and T. Han, Phys. Lett. **212B**, 117 (1988).

[3] V. Barger, T. Han, and R. J. N. Phillips, Phys. Rev. D **39**, 146 (1989).

[4] A. Tofighi-Niaki and J. F. Gunion, Phys. Rev. D **39**, 720 (1989).

[5] M. Golden and S. Sharpe, Nucl. Phys. **B261**, 217 (1985).

[6] F. R. Arutyunian, and V. A. Tumanian, Phys. Lett. 4, 176 (1963); R. H. Milburn, Phys. Rev. Lett. **10**, 75 (1963); see also C. Akerlof, University of Michigan Report No. UMHE 81-59 (1981), unpublished.

[7] I. F. Ginzburg, G. L. Kotkin, V. G. Serbo, and V. I. Telnov, Nucl. Instrum. Methods **205**, 47 (1983); **219**, 5 (1984); V. I. Telnov, Nucl. Instrum. Methods **A294**, 72 (1990).

[8] R. B. Palmer, Annu. Rev. Nucl. Part. Sci. **40**, 529 (1990).

[9] D. L. Burke, "Linear Colliders: When? – How?", to appear in the Proceedings of the XXVI International Conference on High Energy Physics", Dallas (1992).

[10] M. Chanowitz and M.K. Gaillard, Phys. Lett. **142B**, 85 (1984).

[11] We have also checked our results using the analytical amplitudes obtained using REDUCE and FORM. It turned out that the numerical evaluation of cross sections and distributions by the numerical technique is at least ten times faster than the analytical results obtained with REDUCE and FORM.

[12] K. Hagiwara, and D. Zeppenfeld, Nucl. Phys. **B274**, 1 (1986).

[13] G. P. Lepage, J. Comp. Phys. **27**, 192 (1978).

[14] I. F. Ginzburg, G. L. Kotkin, S. L. Panfil, and V. G. Serbo, Nucl. Phys. **B228**, 285 (1983).

[15] M. Baillargeon and F. Boudjema in Proceedings of the "Beyond the Standard Model III", Ottawa, Ontario, June 1992, edited by S. Godfrey (World Scientific).

TABLES

TABLE I. Total cross section in fb for the process $\gamma\gamma \to W^+W^-Z^0$.

$\sqrt{s}$ (GeV)	without cuts	with cuts
500	20.4	10.2
1000	289	81.9

TABLE II. Total cross section in fb for the process $\gamma\gamma \to W^+W^-\gamma$

	$P_T^\gamma > 10$ GeV		$P_T^\gamma > 20$ GeV	
$\sqrt{s}$ (GeV)	without cuts	with cuts	without cuts	with cuts
500	296	115	167	69
1000	1162	192	748	138

FIGURES

FIG. 1. Angular distributions of the vector bosons with the beam pipe. The upper (lower) solid lines stand for the W's, while the upper (lower) dashed line represents the V ($V = Z^0$ or γ) without (with) the cuts discussed in the text. For the $W^+W^-\gamma$ production we imposed the cut $p_T^\gamma > 10$ GeV.

FIG. 2. Rapidity distributions. The conventions are the same as Fig. 1.

FIG. 3. Distributions of the angles between the pair of vector bosons. The upper (lower) solid line stands for the W^+W^- angle while the upper (lower) dashed line represents the WV angle without (with) the cuts discussed in the text. For the $W^+W^-\gamma$ production we imposed the cut $p_T^\gamma > 10$ GeV.

FIG. 4. Invariant mass distributions. The conventions are the same as Fig. 3.

FIG. 5. Energy distributions. The conventions are the same as Fig. 1.

FIG. 6. Transverse momentum distributions. The conventions are the same as Fig. 1.

FIG. 7. Feynman diagrams that contribute to the process $\gamma\gamma \to W^+W^-V$ with $V = Z^0$ or γ.

Fig. 1

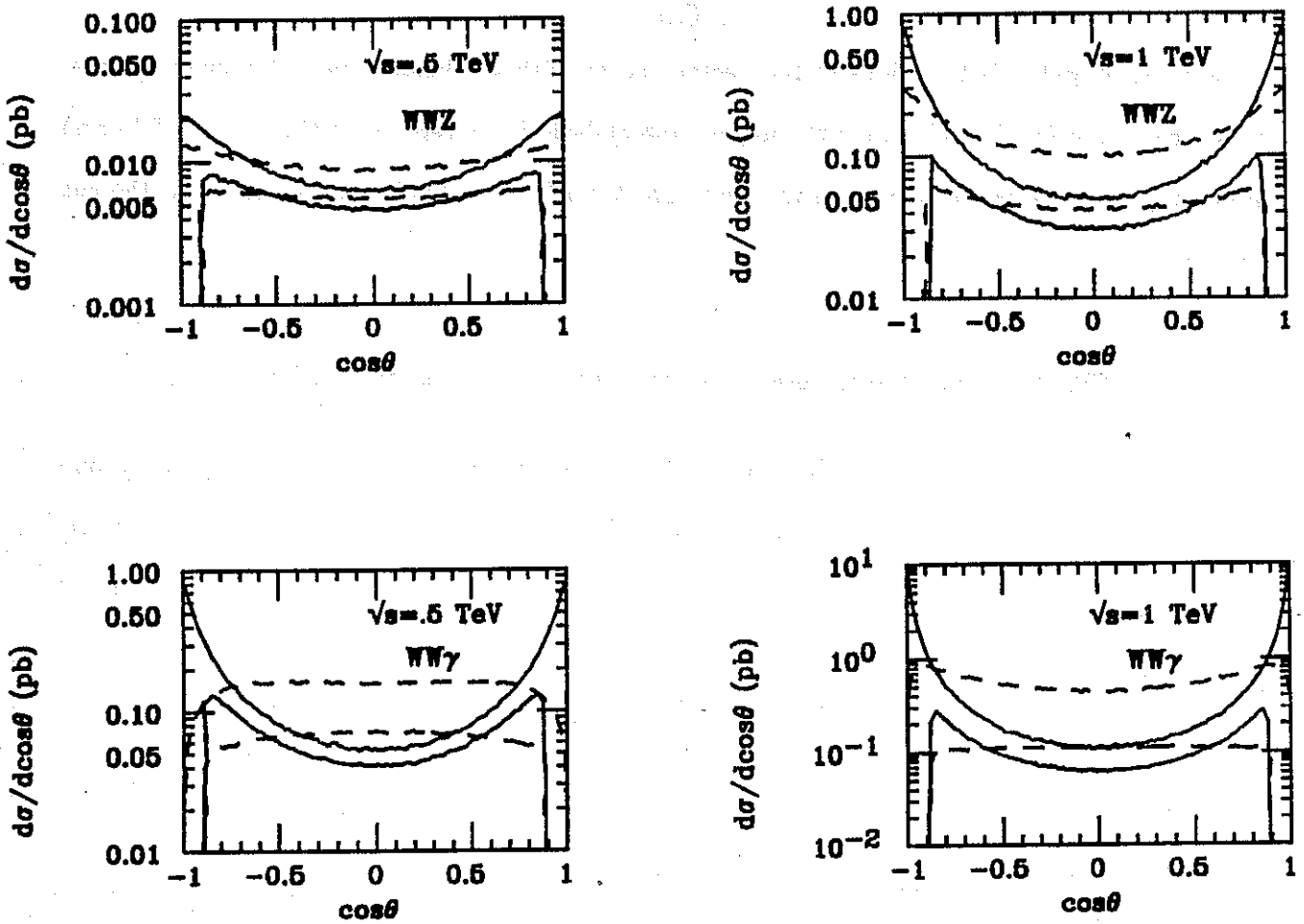
0.100
0.050
0.010
0.005
0.001
√s=.5 TeV
WWZ
dσ/dcosθ (pb)
−1
−0.5
0
0.5
1
cosθ
1.00
0.50
0.10
0.05
0.01
√s=1 TeV
WWZ
dσ/dcosθ (pb)
cosθ
1.00
0.50
0.10
0.05
0.01
√s=.5 TeV
WWγ
dσ/dcosθ (pb)
cosθ
10^1
10^0
10^−1
10^−2
√s=1 TeV
WWγ
dσ/dcosθ (pb)
cosθ

Fig. 2

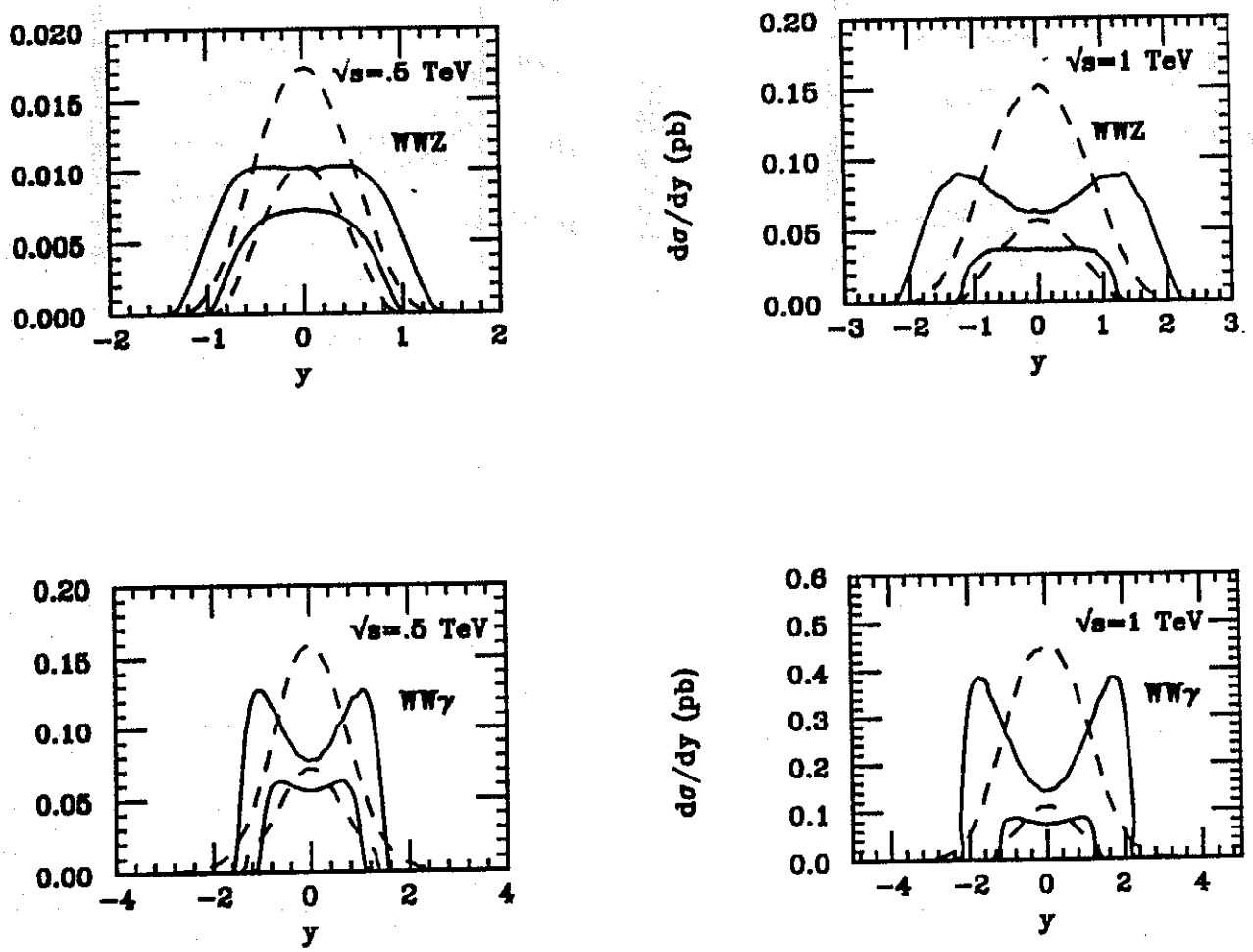

Fig. 3

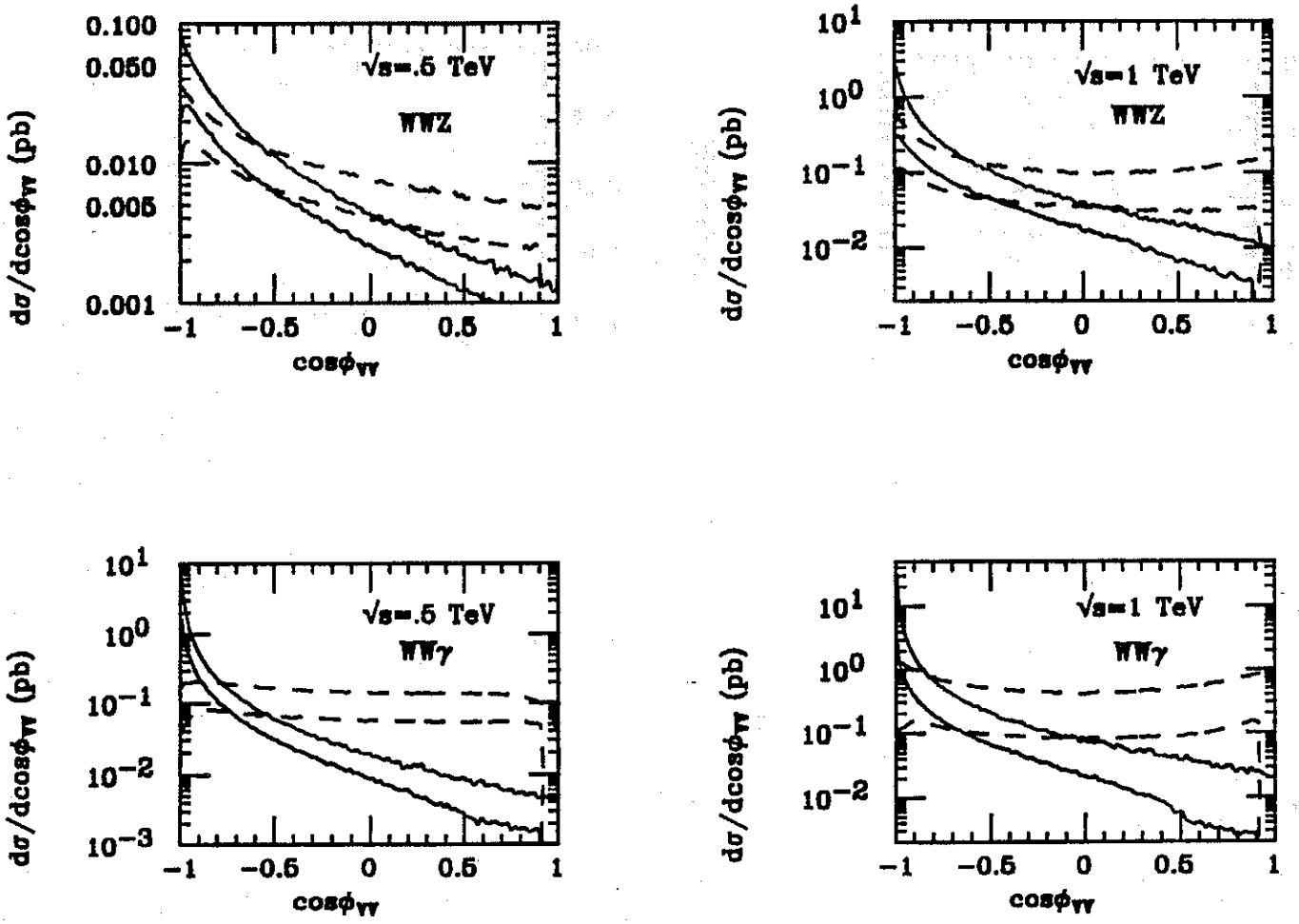
0.100
0.050
0.010
0.005
0.001
√s=.5 TeV
WWZ
dσ/dcosφVV (pb)
−1
−0.5
0
0.5
1
cosφVV
10^1
10^0
10^−1
10^−2
√s=1 TeV
WWZ
dσ/dcosφVV (pb)
cosφVV
10^1
10^0
10^−1
10^−2
10^−3
√s=.5 TeV
WWγ
dσ/dcosφVV (pb)
cosφVV
10^1
10^0
10^−1
10^−2
√s=1 TeV
WWγ
dσ/dcosφVV (pb)
cosφVV

Fig. 4

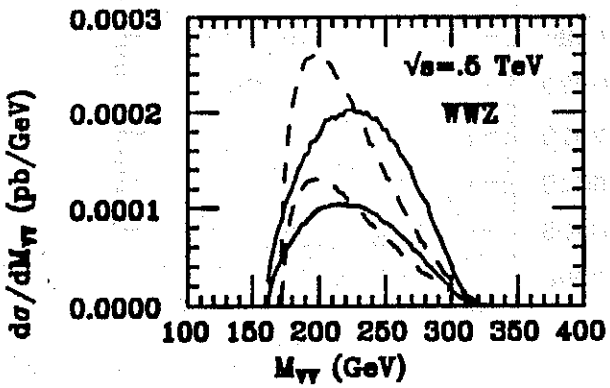
0.0003
0.0002
0.0001
0.0000
√s=.5 TeV
WWZ
dσ/dM_VV (pb/GeV)
100 150 200 250 300 350 400
M_VV (GeV)

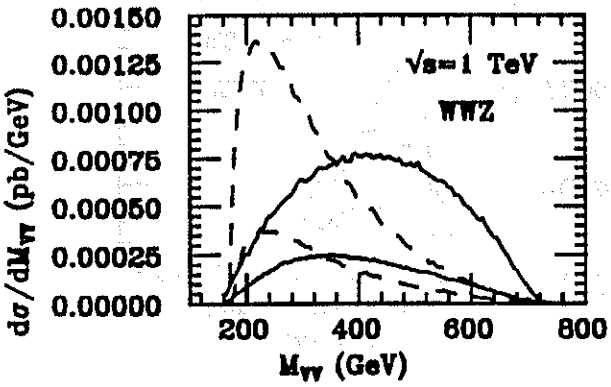
0.00150
0.00125
0.00100
0.00075
0.00050
0.00025
0.00000
√s=1 TeV
WWZ
dσ/dM_VV (pb/GeV)
200 400 600 800
M_VV (GeV)

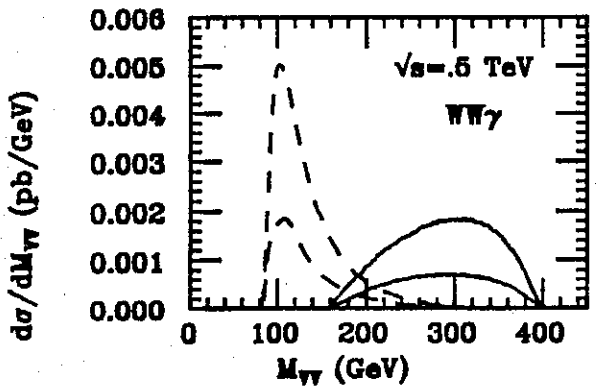
0.006
0.005
0.004
0.003
0.002
0.001
0.000
√s=.5 TeV
WWγ
dσ/dM_VV (pb/GeV)
0 100 200 300 400
M_VV (GeV)

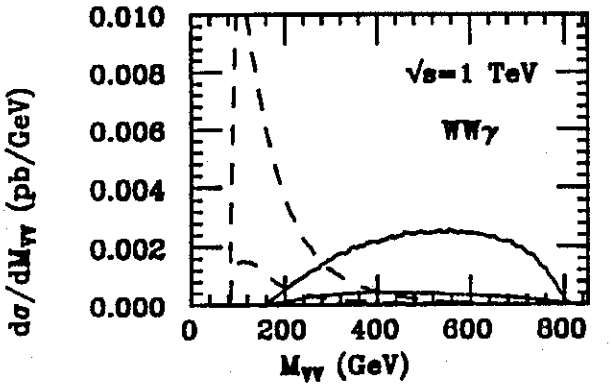
0.010
0.008
0.006
0.004
0.002
0.000
√s=1 TeV
WWγ
dσ/dM_VV (pb/GeV)
0 200 400 600 800
M_VV (GeV)

Fig. 5

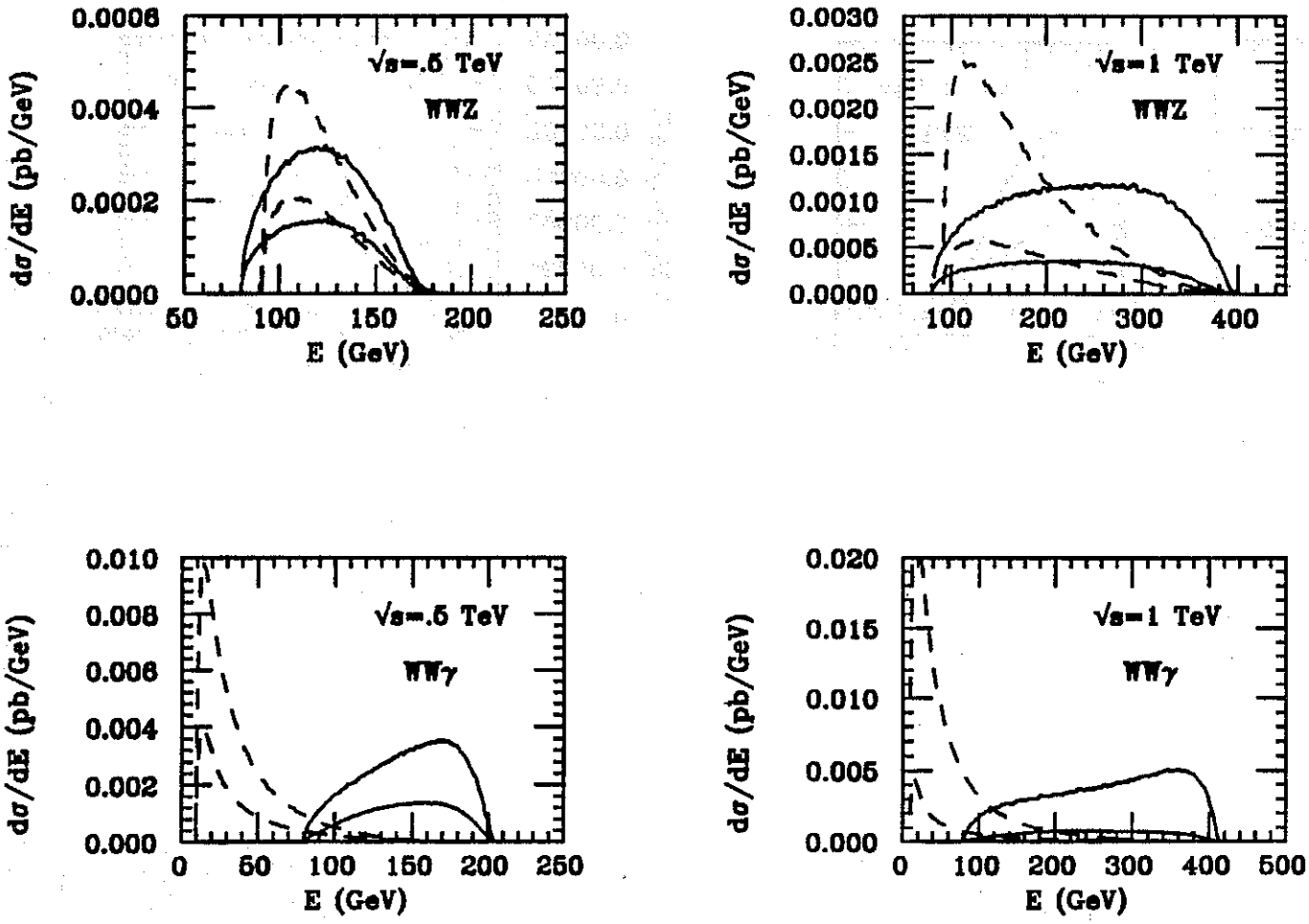

Fig. 6

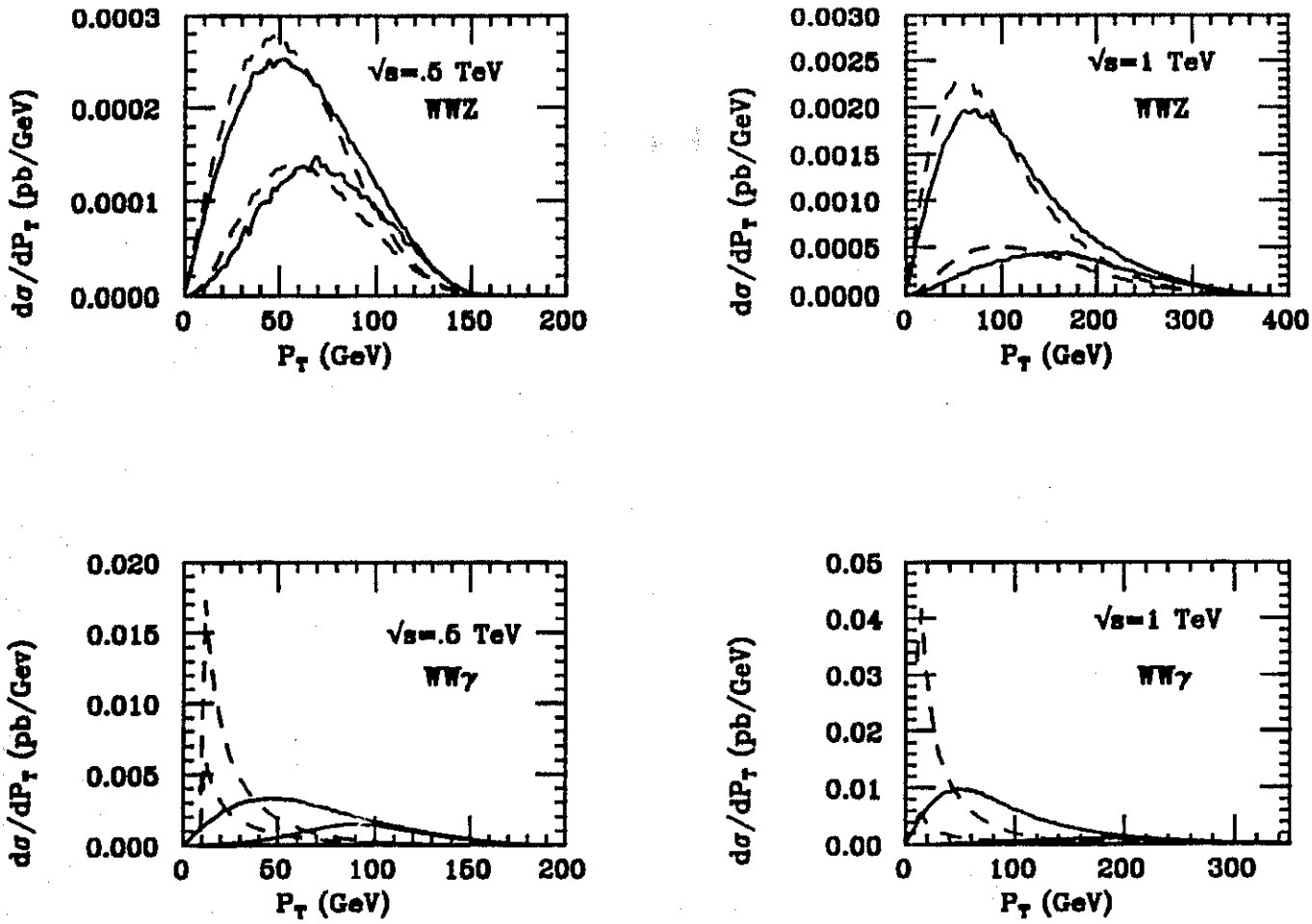
0.0003
0.0002
0.0001
0.0000
dσ/dP_T (pb/GeV)
√s=.5 TeV
WWZ
0
50
100
150
200
P_T (GeV)
0.0030
0.0025
0.0020
0.0015
0.0010
0.0005
0.0000
√s=1 TeV
WWZ
0
100
200
300
400
P_T (GeV)
0.020
0.015
0.010
0.005
0.000
dσ/dP_T (pb/Gev)
√s=.5 TeV
WWγ
0
50
100
150
200
P_T (GeV)
0.05
0.04
0.03
0.02
0.01
0.00
dσ/dP_T (pb/GeV)
√s=1 TeV
WWγ
0
100
200
300
P_T (GeV)

Fig. 7

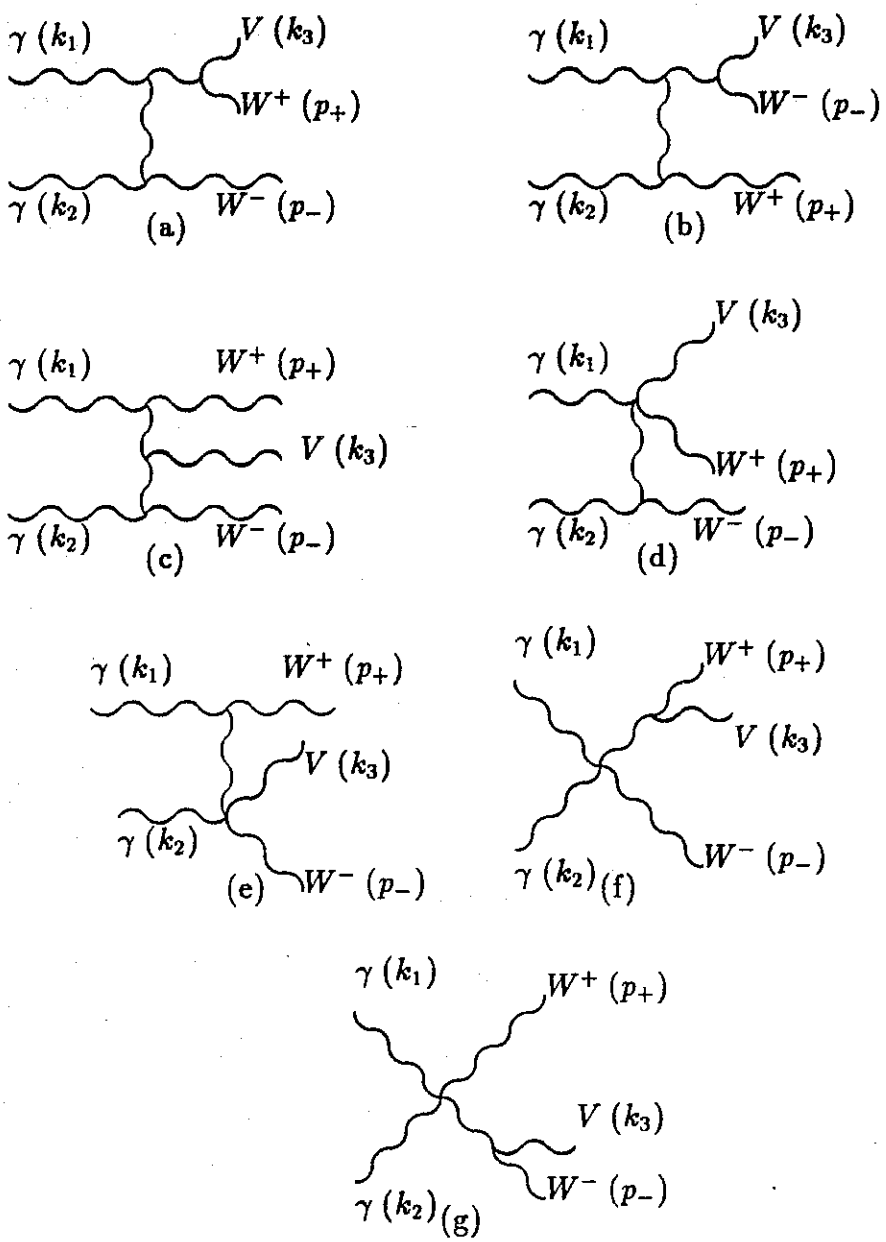

+ crossed diagrams.